RSC Advances

ROYAL SOCIETY
OF CHEMISTRY

www.rsc.org/advances

COMMUNICATION

Loading and Triggered Release of Cargo from Hollow Spherical Gold Nanoparticle Superstructures

Chen Zhang,[a] Thomas Brinzer,[a] Chong Liu,[a] Sean Garrett-Roe,[a] and Nathaniel L. Rosi[a,*]
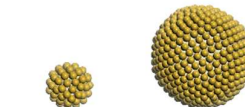
Hollow spherical gold nanoparticle superstructures having different average diameters (~75 nm and ~150 nm) and near-infrared (NIR) extinction were prepared and loaded with an anti-cancer drug, doxorubicin (DOX). The stability of these structures and drug release was monitored in the presence of proteinase and upon irradiation with NIR light. Proteinase K promotes DOX release from the ~150 nm superstructures and NIR light promotes DOX release from both the ~75 nm and ~150 nm superstructures.

Spherical gold nanoparticle assemblies[1-12] having hollow cores and near-infrared (NIR) extinction are of considerable interest because of their potential applications in imaging, drug delivery and photothermal therapy.[2-6] Their exterior surface can be decorated with specific targeting molecules, their hollow interiors can be loaded with therapeutics, and NIR irradiation potentially can be used both to stimulate local heating and to trigger drug release via structural degradation.

We have developed a peptide-based method for assembling gold nanoparticles into hollow spherical gold nanoparticle superstructures.[8,12] This method utilizes peptide conjugate molecules consisting of an inorganic-binding peptide portion derived from phage display and in-vitro selection[13-18] and an assembly-assisting organic moiety.[19-21] The peptide conjugates assemble into spherical soft assemblies and gold nanoparticles assemble onto the outer surface of the assemblies. In previous reports, we demonstrated that C_6-AA-PEP_{Au} ($C_5H_{11}CO$-A-AAYSSGAPPMPPF) can direct the synthesis and assembly of small (~40 nm), medium (~75 nm), and large (~150 nm) spherical gold nanoparticle superstructures. The diameter of the superstructures suggests that the underlying peptide conjugate soft assemblies are vesicular. The medium and large spheres have broad surface plasmon resonance (SPR) extinction, centered at 664 nm and 739 nm respectively, and extending well into the NIR window (Table 1). The hollow vesicular nature of the soft assemblies, their biomolecule-based constitution, the spherical nature of the superstructures, and their NIR extinction properties motivated us to explore whether these materials could be used as carriers for a therapeutic payload.

We first examined the behavior of the spherical superstructures upon irradiation with NIR light. Many nanostructures that absorb in the NIR can be used as antennae for local heating.[22-25] We expected that the medium and large spheres, upon irradiation, would also stimulate local heating; however, we did not know whether the superstructures would remain intact upon irradiation. Large spheres (diameter = 155.4 ± 33.7 nm, based on 100 counts) and medium spheres (diameter = 72.3 ± 15.2 nm, based on 100 counts) were prepared according to our reported method (Fig. 1(a) and (e)).[12]

	Medium Spheres	Large Spheres
Sphere Diameter (nm)	72.3 ± 15.2	155.4 ± 33.7
Nanoparticle Diameter (nm)	8.3 ± 1.6	11.0 ± 2.3
Extinction Maximum (nm)	664	739

Table 1. Structural parameters and extinction maxima for medium and large spherical gold nanoparticle superstructures.

The diameters of the individual gold nanoparticles comprising the large and medium spheres, as determined from transmission electron microscopy (TEM) images, were 11.0 ± 2.3 nm and 8.3 ± 1.6 nm, respectively (each based on 100 counts). Suspensions of the as-synthesized spheres were irradiated with an 805 nm pulsed laser at either 2.59 W (0.52 mJ/pulse, 100 fs fwhm, 5 kHz) or 1.25 W (0.25 mJ/pulse, 100 fs fwhm, 5 kHz) for 10 minutes. The samples were analyzed using TEM before (Fig. 1(a) and (e)) and after irradiation (Fig. 1(b), (c), (f) and (g)). Nearly complete degradation of the large and medium spheres was observed after irradiation at 2.59 W laser power (Fig. 1(b) and (f)). Irradiation at 1.25 W resulted in incomplete degradation (Fig. 1(c) and (g)). Some spheres having ~40-50 nm diameters were observed after irradiation (Fig. 1(c) and (g)). Sphere degradation was also monitored using UV-Vis spectroscopy and the results are consistent with the TEM observations. For both the large and medium spheres, a significant blue shift in the extinction maximum along with narrowing of the

[a.] *Department of Chemistry, University of Pittsburgh, Pittsburgh, Pennsylvania 15260, USA. E-mail: nrosi@pitt.edu*

COMMUNICATION

extinction band was observed after irradiation at 2.59 W, which is consistent with degradation of the assembled superstructures into discrete gold nanoparticles. Less band narrowing and a smaller blue shift was observed for the samples irradiated at 1.25 W, indicating incomplete structure degradation.

Having established that irradiation with the 805 nm laser at 2.59 W was sufficient to degrade the spherical superstructures, we next monitored sphere degradation over time. TEM and UV-Vis data were collected at different time points (2, 4, 6, and 8 min.) during laser irradiation (805 nm, 2.59 W) (Fig. S1, ESI†). These data indicate that the large spheres significantly degrade after 6 min. of irradiation; after 8 min. the sample consists mainly of discrete nanoparticles and some small spheres having average diameters of 42.1 ± 9.5 nm (based on 20 counts). The medium spheres degrade
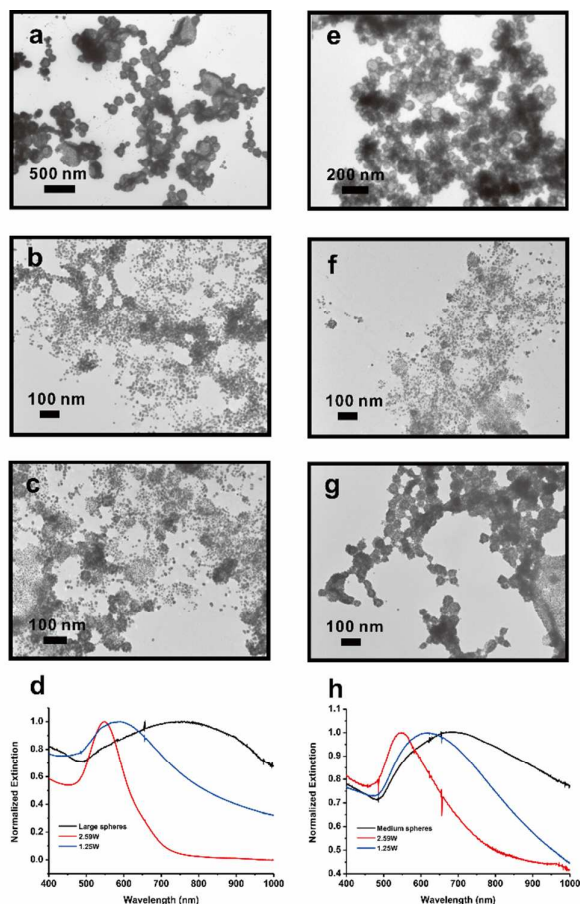

Fig. 1 TEM images of as-synthesized large and medium spheres before (a,e respectively) and after 10 minute irradiation with an 805 nm laser at 2.59 W (b,f respectively) or 1.25 W (c,g respectively). UV-Vis spectra of the as-synthesized large and medium spheres (d,h respectively) before (black line) and after irradiation at the different laser powers (red line, 2.59 W; blue line, 1.25 W).

more slowly; after 8 min. the sample consists of a mixture of discrete nanoparticles and small spheres having average diameters of 43.8 ± 10.0 nm (based on 20 counts). The UV-Vis data are consistent with the TEM observations. After the irradiation degradation experiments, small spheres with diameters of ~40-50 nm remain intact. We note that neither the large or medium sphere

samples are monodisperse, and they contain a distribution of spheres having a range of diameters. The extinction maxima for the spherical superstructures blue shifts with smaller sphere diameter. Spheres having diameters less than ~50 nm are not expected to have a significant extinction at 805 nm;[12,26] therefore, they are not significantly degraded upon irradiation with the 805 nm laser.

Because peptide conjugate molecules are key structural components of the spherical assemblies, it is important to evaluate the stability of the assemblies in the presence of proteases. Ultimately, protease-based degradation could be used for drug release; alternatively, if NIR-triggered release were desired, the spheres should be stable in the presence of protease. The stability of the large and medium spheres was studied in the presence of proteinase K, a non-specific peptidase with a very high specific activity over a wide pH range. First, we monitored the stability of C_6-AA-PEP$_{Au}$ in the presence of proteinase K in HEPES buffer (pH = 7.4). After incubating a solution of C_6-AA-PEP$_{Au}$ for 24 h at 37 °C in the presence of protease K, a sample of the solution was injected into a high performance liquid chromatography (HPLC) instrument. The diagnostic elution peak for C_6-AA-PEP$_{Au}$ was not observed (Fig. S1, ESI†). New peaks are observed at a retention time of 5-6 min., which are likely peptide degradation products. To test the sphere stability, 5 μl of 20 mg/ml proteinase K solution was directly added to the suspension of as-synthesized large and medium spheres and the resulting mixture was incubated at 37 °C for 24h. TEM and UV-Vis spectroscopy were used to monitor sphere stability. Interestingly, we found that proteinase K only causes degradation of the large spheres (Fig. 2(a) and (b)); the medium spheres remain intact after the incubation period (Fig. 2(c) (d)). UV-Vis spectra of the sphere suspensions over the course of 27 h confirm this observation (Fig. 2(e) and (f)). The extinction band for the large spheres disappears over time and a new band at ~540 nm emerges, consistent with the presence of free discrete nanoparticles. The extinction band at 670 nm for the medium spheres blue shifts slightly to 665 nm after 3 h but shows no significant change over the course of 27 h of incubation, indicating that the spheres remain intact. We speculate that the size of the enzyme (~4 nm)[27] is the limiting factor for the enzyme-induced degradation. Although the average observable interparticle distances in the medium spheres (1.4 ± 0.3 nm) and large spheres (1.7 ± 0.5 nm) are both smaller than the size of proteinase K, the medium spheres appear to have more complete and defect-free nanoparticle shells compared to the large spheres, which have some observable defects and areas of incomplete nanoparticle coverage that may allow enzyme entry to the soft peptide-based core.
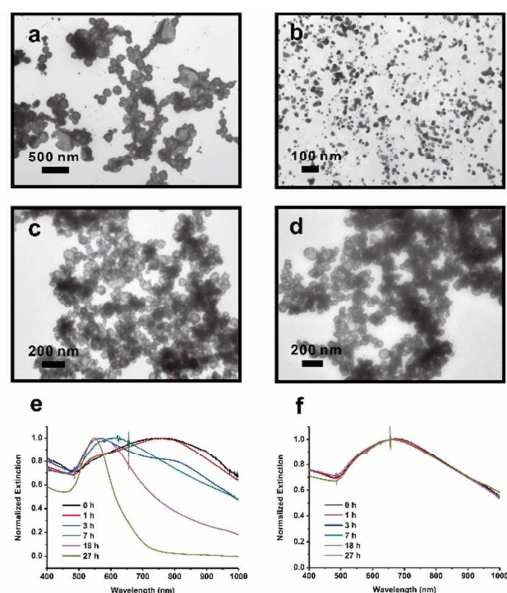
Fig. 2 TEM images of large spheres (a) before and (b) after incubation with proteinase K for one day; TEM images of medium spheres (c) before and (d) after incubation with proteinase K for one day; UV-Vis spectra of (e) large spheres and (f) medium spheres after different incubation times with proteinase K.

We proposed that these spherical nanoparticle superstructures could potentially serve as carriers for therapeutic cargo. To explore this potential application, we chose to load the spheres with the anti-cancer drug, doxorubicin (DOX).[4,5] We attempted to load DOX into the spheres after sphere synthesis (post-synthetic loading) and during sphere synthesis (*in situ* loading). *In situ* loading, in which DOX was added to the sphere synthesis, proved to be more effective (see ESI for loading details). TEM was used to confirm the formation of spheres in the presence of DOX. The average diameters of the large and medium spheres were 152.3 ± 32.8 nm and 74.5 ± 14.6 nm (each based on 100 counts), respectively (Fig. S3(a) and (b), ESI†), which is comparable to the sphere diameters in the absence of DOX. The amount of loaded DOX, or loading efficiency, was determined by calculating the difference between the amount of DOX added to the synthesis and the amount of DOX washed out after loading (see ESI for details). UV-Vis was used to quantify DOX. The loading efficiency, expressed as the percentage of total DOX added to the syntheses, was 51% for large spheres and 43% for medium spheres. These loading percentages were significantly larger than what was observed for drug loading *after* sphere synthesis. In those cases, we observed loading efficiencies of only 4% and 2% for the large and medium spheres, respectively. The post-synthetic loading amounts likely reflect physical absorption of DOX onto the sphere exterior while the *in situ* loading reflects incorporation of DOX into the sphere interior during synthesis. We also measured DOX fluorescence before and after loading using the two different loading methods. Very little quenching of DOX fluorescence was observed for the post-synthetic loading while significant quenching was observed for the *in situ* loading (Fig. S3(c) and (d), ESI†). DOX fluorescence is quenched when it is in proximity to the gold nanoparticles. More quenching is observed for the large spheres compared to the medium spheres, which is consistent with the DOX loading efficiency calculated using by UV-Vis spectroscopy. We note that a portion of the observed

quenching is likely from self-quenching due to the high local concentration of DOX within the spheres.[28]

After preparing the DOX-loaded spheres, DOX leakage from the spheres was monitored. The loaded spheres were washed and isolated via centrifugation (see ESI for details). First, the spheres were suspended in either 0.1 M HEPES buffer (pH = 7.4) or 0.1 M PBS buffer (pH = 7.4). Cumulative DOX leakage at different time points was measured. Briefly, at each time point, the suspension was centrifuged, and the supernatant was analyzed for DOX using UV-Vis spectroscopy. After each time point, the remaining solid was re-dispersed in fresh buffer. DOX leakage was observed for both large spheres and medium spheres in both HEPES buffer and PBS buffer (Fig. S4(a) and (b), ESI†). The cumulative release profiles indicate continuous leakage within the first 9 h for both large spheres and medium spheres in both HEPES buffer and PBS buffer. In both buffers. After 32 h, the final cumulative leakage for large spheres and medium spheres are ~17% and ~13% in HEPES buffer and ~16% and ~14% in PBS buffer, respectively. Since tumor tissues are usually acidic due to hypoxia,[29] DOX leakage was also monitored in acetate buffer (pH = 5.0) to determine whether acidic conditions would lead to DOX release (Fig. S4(c), ESI†). However, the results of these studies are similar to those for HEPES buffer and PBS buffer. In acetate buffer, the final cumulative leakage for large spheres and medium spheres are ~20% and ~16%, respectively, indicating that an acidic environment does not lead to increased DOX release. Collectively, these experiments demonstrate that the majority of loaded DOX remains within the spheres upon storage in buffer.

Next, two mechanisms of DOX release from the spherical superstructures were explored: enzyme-triggered release and NIR-triggered release. Having demonstrated that large spheres degrade in the presence of proteinase K whereas medium spheres are stable, we tested whether proteinase K would have similar effects on the DOX-loaded spheres. 5 µl of 20 mg/ml proteinase K was directly added to the DOX-loaded spheres suspended in either 0.1 M HEPES (pH = 7.4) or 0.1 M PBS buffer (pH = 7.4). Thereafter, the mixtures were incubated at 37 °C for up to 32 h. DOX release profiles were determined by measuring the absorption of free DOX (485 nm) in the supernatant after centrifugation (Fig. 3). The release profile for the large spheres in HEPES buffer (Fig. 3(a)) exhibits three distinct regions: i) an initial release period from 0-~2.5 hrs during which ~15 % of loaded DOX is released; ii) an intermediate period of rapid DOX release between ~2.5 h and ~7 h, after which ~70% of loaded DOX is released; and a final period of very gradual DOX release between ~7 h and 32 h. A cumulative DOX release of ~73% is observed after 32 h. The release profile in PBS buffer was comparable to that observed in HEPES buffer. DOX release in the initial period is likely due to leakage from the spheres, because the amount released and the rate of release are similar to what was observed for the leakage experiments. Recalling that significant degradation of the large spheres was observed by 3 h of incubation with proteinase K (Fig. 2(e)), we can attribute the onset of the second rapid DOX release period at ~2.5 h to proteinase K induced sphere degradation. The third gradual release period may be due to slow desorption of DOX from nanoparticle surfaces. The remaining ~27% of loaded DOX likely remains associated with the nanoparticle pellet after centrifugation. In contrast, DOX-loaded medium spheres show only limited release within the first ~6 hours and a final cumulative DOX release of 15%, which is comparable to the amount of DOX released in HEPES buffer and PBS buffer during the leakage tests (Fig. 3(a)). Therefore, we attribute this observed release to leakage rather than degradation of the superstructure. Fluorescence spectroscopy was also used to monitor the release of

DOX from the drug-loaded spheres in the presence of proteinase K (Figure S5(a) and (b), ESI†). These data are consistent with the results obtained from UV-Vis experiments: for the large spheres, the fluorescence intensity increases dramatically during the first 7 h and then gradually increases over the next 20 h; for the medium spheres, the fluorescence intensity shows only a slight increase over the course of 27 hours. Collectively, these results indicate that DOX-loaded medium spheres are stable in the presence of enzyme and that enzymes can be used to trigger DOX release from the DOX-loaded large spheres.
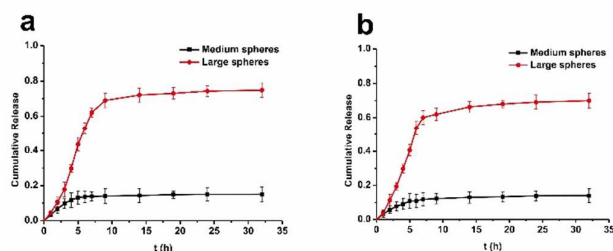

Fig. 3. Cumulative DOX release profile for the large spheres and medium spheres upon incubation with proteinase K in (a) HEPES buffer (pH = 7.4) and (b) PBS buffer (pH = 7.4).

NIR radiation was explored as a second alternative method for triggering the release of DOX from the DOX-loaded large and medium spheres. DOX-loaded sphere samples were irradiated with an 805 nm laser at 2.49 W for 10 minutes. UV-Vis spectroscopy was used to determine that 82% and 69% of the loaded DOX was released from the large spheres and medium spheres, respectively, after laser irradiation. TEM images reveal sphere degradation (Fig. 4(a) and (b)). Fluorescence spectra of the DOX-loaded spheres collected before and after irradiation provide further proof of DOX release (Fig. 4(c) and (d)). The observed fluorescence intensity for DOX increases after irradiation, which is expected once the DOX molecules are released from the spheres and are no longer in proximity to the gold nanoparticles. Taken together, all of these results indicate laser irradiation can effectively trigger DOX release from both the large and medium spheres.
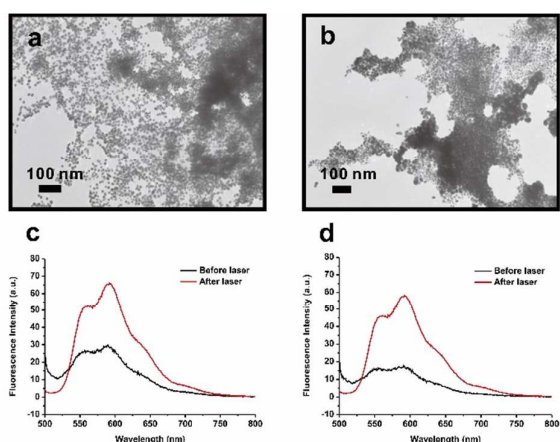

Fig. 4. TEM images of DOX-loaded (a) large spheres and (b) medium spheres after laser irradiation at 805 nm for 10 minutes. Fluorescence spectra of DOX-loaded (c) large spheres

and (d) medium spheres before and after laser irradiation at 805 nm for 10 minutes.

Conclusions

In summary, we have successfully prepared spherical gold nanoparticle superstructures and loaded these structures with DOX. The spheres exhibit size-dependent stability in the presence of proteinase K. DOX release from the large spheres can be triggered via degradation with proteinase K, and DOX release from both the large and medium spheres can be triggered via irradiation with NIR light. These studies represent the first step toward using these biomolecule-based nanoparticle superstructures as carriers of therapeutic cargo for biomedicine applications. Current work is focused on achieving more efficient drug loading, preventing leakage of drug, designing spheres that degrade in the presence of sequence-specific proteases, and proceeding with *in vitro* studies.

Acknowledgement

References

1   J. Hu, T. Wu, G. Zhang and S. Liu, *Journal of the American Chemical Society*, 2012, **134**, 7624-7627.
2   J. He, X. Huang, Y.-C. Li, Y. Liu, T. Babu, M. A. Aronova, S. Wang, Z. Lu, X. Chen and Z. Nie, *Journal of the American Chemical Society*, 2013, **135**, 7974-7984.
3   J. Song, L. Cheng, A. Liu, J. Yin, M. Kuang and H. Duan, *Journal of the American Chemical Society*, 2011, **133**, 10760-10763.
4   J. Song, L. Pu, J. Zhou, B. Duan and H. Duan, *ACS Nano*, 2013, **7**, 9947-9960.
5   J. Song, J. Zhou and H. Duan, *Journal of the American Chemical Society*, 2012, **134**, 13458-13469.
6   J. He, Z. Wei, L. Wang, Z. Tomova, T. Babu, C. Wang, X. Han, J. T. Fourkas and Z. Nie, *Angewandte Chemie*, 2013, **125**, 2523-2528.
7   J. He, Y. Liu, T. Babu, Z. Wei and Z. Nie, *Journal of the American Chemical Society*, 2012, **134**, 11342-11345.
8   L. Hwang, G. Zhao, P. Zhang and N. L. Rosi, *Small*, 2011, **7**, 1939-1942.
9   C. Song, G. Zhao, P. Zhang and N. L. Rosi, *Journal of the American Chemical Society*, 2010, **132**, 14033-14035.
10 K. Niikura, N. Iyo, T. Higuchi, T. Nishio, H. Jinnai, N. Fujitani and K. Ijiro, *Journal of the American Chemical Society*, 2012, **134**, 7632-7635.
11 M. R. Rasch, E. Rossinyol, J. L. Hueso, B. W. Goodfellow, J. Arbiol and B. A. Korgel, *Nano Letters*, 2010, **10**, 3733-3739.

12 C. Zhang, Y. Zhou, A. Merg, C. Song, G. C. Schatz and N. L. Rosi, *Nanoscale*, 2014, **6**, 12328-12332.

13 S. R. Whaley, D. S. English, E. L. Hu, P. F. Barbara and A. M. Belcher, *Nature*, 2000, **405**, 665-668.

14 J. M. Slocik, M. O. Stone and R. R. Naik, *Small*, 2005, **1**, 1048-1052.

15 D. B. Pacardo, M. Sethi, S. E. Jones, R. R. Naik and M. R. Knecht, *ACS Nano*, 2009, **3**, 1288-1296.

16 C.-Y. Chiu, Y. Li, L. Ruan, X. Ye, C. B. Murray and Y. Huang, *Nat Chem*, 2011, **3**, 393-399.

17 M. B. Dickerson, K. H. Sandhage and R. R. Naik, *Chemical Reviews*, 2008, **108**, 4935-4978.

18 C.-L. Chen and N. L. Rosi, *Angewandte Chemie International Edition*, 2010, **49**, 1924-1942.

19 J. D. Hartgerink, E. Beniash and S. I. Stupp, *Science*, 2001, **294**, 1684-1688.

20 J. D. Hartgerink, E. Beniash and S. I. Stupp, *Proceedings of the National Academy of Sciences*, 2002, **99**, 5133-5138.

21 S. E. Paramonov, H.-W. Jun and J. D. Hartgerink, *Journal of the American Chemical Society*, 2006, **128**, 7291-7298.

22 X. Huang, I. H. El-Sayed, W. Qian and M. A. El-Sayed, *Journal of the American Chemical Society*, 2006, **128**, 2115-2120.

23 J. Nam, N. Won, H. Jin, H. Chung and S. Kim, *Journal of the American Chemical Society*, 2009, **131**, 13639-13645.

24 S. Lal, S. E. Clare and N. J. Halas, *Accounts of Chemical Research*, 2008, **41**, 1842-1851.

25 L. Au, D. Zheng, F. Zhou, Z.-Y. Li, X. Li and Y. Xia, *ACS Nano*, 2008, **2**, 1645-1652.

26 M. Chandra, A.-M. Dowgiallo and K. L. Knappenberger, *Journal of the American Chemical Society*, 2010, **132**, 15782-15789.

27 C. Betzel, G. P. Pal and W. Saenger, *European Journal of Biochemistry*, 1988, **178**, 155-171.

28 Z. S. Al-Ahmady, W. T. Al-Jamal, J. V. Bossche, T. T. Bui, A. F. Drake, A. J. Mason and K. Kostarelos, *ACS Nano*, 2012, **6**, 9335-9346.

29 I. F. Tannock and D. Rotin, *Cancer Research*, 1989, **49**, 4373-4384.